Electrochimica Acta 248 (2017) 197–205

Contents lists available at ScienceDirect

Electrochimica Acta

journal homepage: www.elsevier.com/locate/electacta

A highly active biomass-derived electrode for all vanadium redox flow batteries

Z.H. Zhang[a,b], T.S. Zhao[b,*], B.F. Bai[a], L. Zeng[b,c], L. Wei[b]

[a] State Key Laboratory of Multiphase Flow in Power Engineering, Xi'an Jiaotong University, Xi'an 710049, China
[b] Department of Mechanical and Aerospace Engineering, The Hong Kong University of Science and Technology, Clear Water Bay, Kowloon, Hong Kong, China
[c] HKUST Jockey Club Institute for Advanced Study, The Hong Kong University of Science and Technology, Clear Water Bay, Kowloon, Hong Kong SAR, China

ARTICLE INFO

Article history:
Received 26 April 2017
Received in revised form 8 July 2017
Accepted 21 July 2017
Available online 24 July 2017

Keywords:
Vanadium flow battery
Biomass electrode
Cotton
Surface area
Catalytic activity

ABSTRACT

In this work, we report an environmentally friendly and low-cost approach to synthesize an all biomass-derived electrode from cotton through a pyrolysis process and apply this novel electrode to a VRFB for the first time. It is demonstrated that this carbonized cotton (CC) electrode presents a higher BET surface area, a larger number of oxygen-containing functional groups, a better wettability and higher catalytic activity for vanadium reactions than commercial carbon papers (CPs) do. As a result, the CC electrode improves the reversibility toward VO^{2+}/VO_2^+ by 100 mV lower peak separation as compared with commercial CPs. Moreover, the VRFB assembled with the prepared electrodes delivers a high voltage efficiency of 75.4% at a current density of 100 mA cm^{-2}, outperforming the oxidized CPs (68.3%), and a better rate performance during the charge-discharge test at various current densities. These results suggest that the carbonized cotton electrode offers a great promise for the large-scale application in VRFBs.

1. Introduction

The gradual depletion of traditional fossil fuels and the increasing environmental pollution have promoted the rapid development of clean and sustainable energy sources, such as solar and wind energy [1]. However, the renewable energy sources encounter many issues during their applications, for instance, intermittence, distribution and fluctuation [1,2]. The energy storage systems such as redox flow batteries (RFBs), therefore, are developed to attenuate the mismatch between the supply and demand of electricity [3,4]. Among various RFBs, all vanadium redox flow batteries (VRFBs) proposed by Skyllas-Kazacos have received extensive attention due to their attractive features of design flexibility, long lifespan and decoupled power and energy capacity [1,5]. In particular, VRFBs employ the same element (vanadium) in both positive and negative electrolytes to minimize the cross-contamination, thereby resulting in a long cycle life and high energy efficiency [6].

Despite their compelling merits, a critical issue that hampers the commercialization of VRFBs is the high capital cost. In this regard, a VRFB capable of operating under high charge/discharge current density is highly desired, mainly because the improved power density can lead to a reduced stack size, thus achieving a much lower capital cost of the system [7]. However, the large polarization at higher current densities in flow battery is a critical issue in attaining a high efficiency and rate capability. Normally, the overall polarization consists of ohmic polarization, activation polarization, and concentration polarization. These polarizations are largely affected by the morphology and surface chemistry of electrode materials [7–9]. Therefore, many researchers have focused on developing effective electrode materials to reduce the cell overpotential.

The electrodes in VRFB system are mainly carbonaceous materials owing to their high electrical conductivity, good stability, corrosion resistance and a wide range of operating potential [8,10,11]. Thereinto, graphite felts and carbon papers, which are generally derived from polyacrylonitrile (PAN) processed at ultra high temperatures (>2000 °C), are the most widely-used electrodes in VRFBs. Nevertheless, the intrinsic poor electrochemical activity and bad wettability of these electrodes deliver an inert electrochemical reaction and mass transfer process, inducing a

* Corresponding author.
E-mail address: metzhao@ust.hk (T.S. Zhao).

http://dx.doi.org/10.1016/j.electacta.2017.07.129
0013-4686/

large activation loss during the course of battery operation [12,13]. Moreover, relatively high cost is another issue should be concerned in large-scale commercial application [14–16]. To overcome the aforementioned drawbacks, a variety of approaches including thermal treatments, plasma treatments, electrochemical activation and hydrothermal treatment [17–22] have been performed on commercial carbon electrodes to improve the wettability of electrodes and enhance the catalytic effect for vanadium redox reactions. Nevertheless, these surface modifications showed limited improvement on the battery performance owing to the relatively low surface area [23]. Recently, carbon electrocatalysts such as CNTs, graphene and carbon nanofibers [24–30] have been suggested as effective candidates by depositing on electrodes and have led to outstanding cell performance owing to their high surface area and good electric conductivity. Besides, metal oxides (Mn_3O_4, TiC, WO_3 and Nb_2O_5) [30–34] have also been reported as catalysts to promote the vanadium redox reaction. However, these approaches may be not suitable for practical applications due to the harsh synthesis conditions, high price of metal precursors or limited enhancement of battery performance [29]. It is worth mentioning that the low-cost catalysts (ZrO_2, CeO_2) [23,35] were synthesized through a facile precipitation method and have displayed a highly improved performance in VRFBs. More recently, the electrospun carbon nanofibers with nanoparticle catalysts [36,37] were reported as novel electrodes and exhibited good performance in VRFB due to their attractive features of large surface area, high electron conductivity and electrocatalytic activity. Nevertheless, to implement the large-scale application, developing more cost-effective and mass-produced electrodes through a facile way may be of great importance for VRFBs in the near future.

In the past decades, biomass-derived materials have gained much attention and are widely used in energy devices such as supercapacitors and lithium batteries owing to their advantages of light weight, flexibility and low cost [38–43]. However, few efforts have been reported for redox flow batteries till now. Very recently, Srinivasan et al. demonstrated that the mesoporous carbon derived from coconut shell had good catalytic effect for the V(II)/V(III) redox reaction [44]. Besides, corn protein-derived nitrogen-doped carbon materials synthesized by Park et al. were also reported as effective catalyst for VRFBs [45]. In their work, the biomaterials were ground into powders and converted to functional nanoparticles after a series of complex synthesis procedures including hydrothermal process and thermal treatment, then the conventional graphite felt decorated with the aforementioned nanoparticles with Nafion as binder was applied in VRFB. That was to say, the biomaterials just took effect as the supported catalysts and the electrodes used in their work were still restricted to conventional graphite felt and carbon felt. Up to now, all biomass-derived electrodes have not been reported in VRFBs yet.

Hence, we want to fabricate a flexible and integrated electrode from biomass material that can be directly applied in VRFBs. The natural cotton, as an inexpensive, high-yielding and environment-friendly plant material consisting of cellulose fibers, can serve as precursor to prepare novel electrode due to the low preparation cost, simple preparation process and high production. In this work, we fabricated a new biomass-derived electrode through a facile carbonization process from the natural cotton and denoted it as carbonized cotton (CC) electrode. After pyrolysis, the CC electrode showed a porous structure interconnected with the carbonized fibers, similar with commercial graphite felts, but presented a much larger surface area. Furthermore, the CC electrode exhibited excellent hydrophilicity and electrochemical activity due to the abundant oxygen functional groups on the surface of the fibers, which were beneficial to reduce the concentration and kinetic overpotentials. The CC electrode was then applied in a VRFB system and found to deliver a good performance. To the best of our knowledge, this is the first attempt to use all bio-derived material as an integrated electrode in VRFBs. Comprehensive characterizations and electrochemical studies of this new electrode were performed and described in detail.

2. Experimental

2.1. Preparation of cotton-based electrode

The pristine cotton pads purchased from Watsons with non-woven fabric structure were adopted as precursor materials in this work. The raw cotton, used as received, were pyrolyzed at 1000 °C for 1 h with a heating rate of 5 °C min^{-1} in a quartz tube furnace with a flow of inert argon gas. The cotton-derived electrode with the thickness of about 300–400 μm was denoted as carbonized cotton (CC) electrode. Carbon papers (SGL-10AA 300 μm) and oxidized carbon papers which were thermally treated in air at 400 °C for 6 hours, were prepared for comparison and denoted as CP and oxidized CP electrodes respectively. Afterwards, all of these samples were cut into pieces of 2 cm × 2 cm for further usage.

2.2. Physical characterization and electrochemical tests

The morphologies of the prepared CC electrode were observed using a scanning electron microscope (SEM, JEOL-6700F) at an acceleration voltage of 10 kV. Transmission electron microscopy (TEM) images of the carbonized fiber from CC electrode were collected in a high-resolution JEOL 2010F TEM system at 200 kV. For TEM observation, the samples were dispersed in ethanol, sonicated and dripped onto the holey carbon-coated Cu grids. X-ray diffraction (XRD) patterns of CC, CP and oxidized CP electrodes were obtained on XRD system (model PW 1825) with the angle range from 10° to 70° with scanning rate of 5° min^{-1}. Raman spectra were recorded by Renishaw RM 3000 with 532 nm laser. The Brunauer-Emmett-Teller (BET) surface area and pore distribution of CC, CP and oxidized CP were determined *via* nitrogen adsorption-desorption method at 77 K after the degassing process at 150 °C for 180 min. X-ray photoelectron spectroscopy (XPS) was performed using a Physical Electronics PHI 5600 multi-technique system equipped with an Al monochromatic X-ray source at a power of 350 W to study the surface chemical state. In addition, the wettability of all electrodes was analyzed by the contact angle tester.

Cyclic voltammetry (CV) and electrochemical impedance spectroscopy (EIS) were conducted in a three-electrode cell in which platinum mesh and Ag/AgCl were used as the counter and reference electrodes, respectively. The CC, CP and oxidized CP samples with a diameter of 5 mm punched from the prepared electrodes were used as working electrodes. Before testing, the working electrodes were immersed in the electrolyte and air bubbles were removed in a vacuum chamber. The CV tests were carried out between 0.0 V and 1.4 V at 5 mV s^{-1} in 1 M $VOSO_4$ + 3 M H_2SO_4 and AC impedance was measured in a frequency range from 10^{-2} to 10^5 Hz with an amplitude of 5 mV at the open circuit potential.

2.3. Single cell test

To further demonstrate the practical application of the prepared CC material, the single cells with various electrodes were assembled for the charge-discharge tests. The CC, CP and oxidized CP with the active area of 4 cm^2 were used as both positive and negative electrodes. Nafion 212 was employed as the separator and placed between two electrodes. Two pieces of graphite plates with parallel flow fields, copper current collectors, and stainless steel

end plates were assembled. The WT600-2J pump with pump heads of YZ1515X (Baoding Longer Precision Pump Co., Ltd) was used for pumping electrolytes. At the beginning of the test, 25 ml 1 M V(IV) in 3 M H_2SO_4 solution and 25 ml 1 M V(III) in 3 M H_2SO_4 solution were pumped into the positive side and negative side respectively with a flow rate of 46 mL min^{-1} (60 rpm). The charge-discharge test was carried out at different current densities of 40, 60, 80 and 100 mA cm^{-2}. The cut-off voltage was set as 1.65 V for charge process and 0.9 V for discharge process.

3. Results and discussion

Fig. 1a visually shows the morphologies of the cotton pad before and after carbonization. The pristine cotton has a rectangle structure (10 cm × 6.5 cm) with a weight of 0.80 g. After thermal annealing, the white cotton pad is converted to the black CC electrode with a shrunken area of 5.5 cm × 4 cm and a largely reduced weight of 0.11 g. For one piece of electrode used in the battery with the size of 2cm × 2 cm, the carbonized cotton electrode has a weight of 0.02 g, which is lighter than one piece of carbon paper (0.03 g). Fig. 1b shows that the CC electrode can be folded into various multilayer structures, stating that the direct conversion of cotton into carbonized cotton by simple thermal treatment maintains its mechanical property and flexibility. The morphologies of the cellulose fibers in the raw cotton, as presented in SEM image of Fig. 1c, are shaped like curled strips with the diameters ranging from a few micrometers to tens of micrometers. After the pyrolysis process, the carbonized microfibers are much thinner than the pristine fibers and show the partially helical and twining morphologies, as illustrated in Fig. 1d, indicating that the fibrous frameworks undergo an obvious shrinkage during carbonization due to burn-off of the non-carbon elements and carbon-containing compounds. However, the 3D carbon framework of the cotton-derived electrode is well-preserved, which allows the electrolyte to deliver fast ion transport in the porous structure. The typical high-resolution individual fibers are presented in Fig. 1e and f, it can be seen many wrinkles formed on the surface during the pyrolysis process, thus providing a larger surface area. More interestingly, a tubular character of the fiber can be seen from the hollow structure of the cross profile, as shown in Fig. 1f.

Fig. 2a is a typical low magnification TEM image showing the morphology of the carbonized cotton fiber. Although the tube wall is very thick for the electron transmission, the tubular structure of the fiber can still be observed with the inner diameter of 1 μm and wall thickness of 0.5 μm. The high magnification image in Fig. 2b clearly shows a higher crystallinity layer at the inner part which

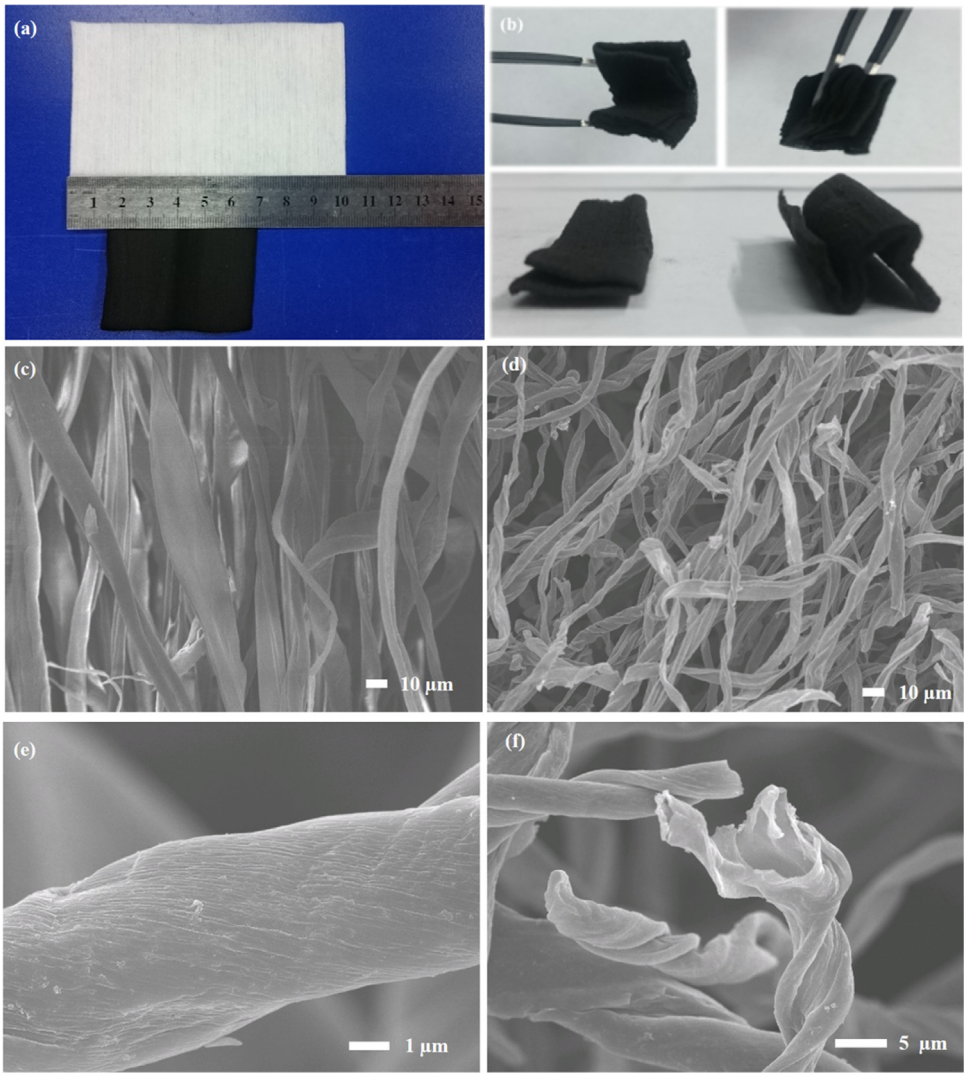

Fig. 1. (a) The photograph of the pristine cotton pad and carbonized cotton (CC); (b) Excellent mechanical flexibility of CC electrode in different folded states; SEM images of (c) pristine cotton and (d) CC; SEM images of (e) the surface of individual carbonized cellulose fiber and (f) cross profile of carbonized fibers.

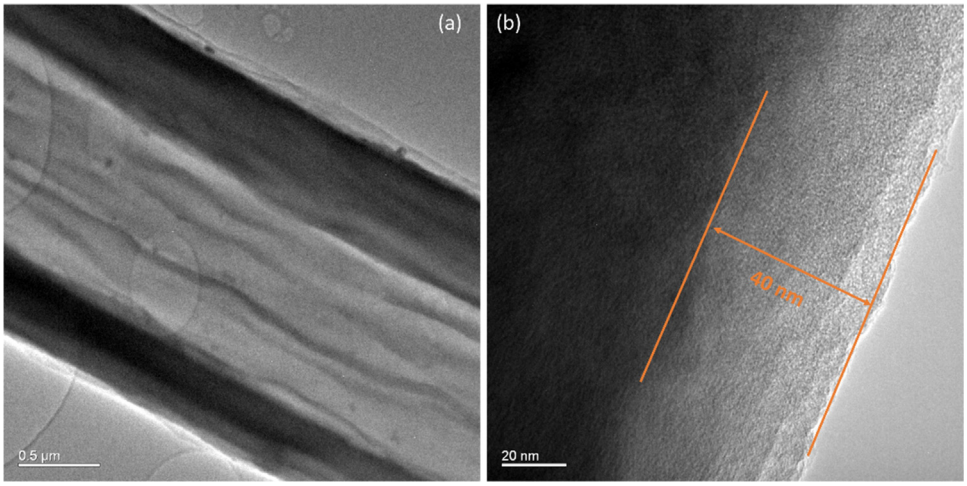

Fig. 2. A typical TEM morphology of an individual carbonized cotton fiber (a) and the corresponding high-resolution TEM image (b).

serves as the effective pathway for electron transport, and a 40 nm thick amorphous carbon layer at the outer edge, which provides adequate active sites due to the large amounts of defects and functional groups.

XRD and Raman were also conducted to further study the microstructure of the samples. As illustrated in Fig. 3a, the XRD patterns for CP and oxidized CP show a significant diffraction peak located at 26.4° and two weak diffraction peaks at about 43.6° and 54.3°, corresponding to the (002), (100) and (004) planes of graphitic carbon, respectively. The XRD peaks for CC exhibit a lower diffraction intensity due to the amorphous carbon and structure defects on the surface. However, two broad peaks at $2\theta = 26.4°$ and 43.1° observed in the enlarged figure suggest the formation of graphitic carbon in the carbonized fiber. The Raman spectra of CC, CP and oxidized CP (Fig. 3b) present a D-band and a G-band at around 1340 cm^{-1} and 1580 cm^{-1}, corresponding to the disordered carbon defects and graphitized carbon structure in the carbonaceous materials, respectively [46]. The integrated intensity ratio of D-band to G-band (I_D/I_G) is used to estimate the crystallinity of carbon materials. The I_D/I_G values for CP and oxidized CP were 0.80 and 0.86 respectively, revealing a highly graphitic structure of commercial electrode materials. The CC electrode had a larger I_D/I_G value of 1.05 because of the amorphous structure and abundant defects. Nevertheless, there was still much sp^2 type carbon formed in CC, which presented a relatively high graphitization and good electric conductivity [47].

BET measurements were performed and the nitrogen adsorption-desorption isotherms and pore size distribution curves of all samples are given in Fig. 3c and d. As presented in Fig. 3c, the pronounced hysteresis loop in the range of 0.40-0.99 P/P_0 for CC is

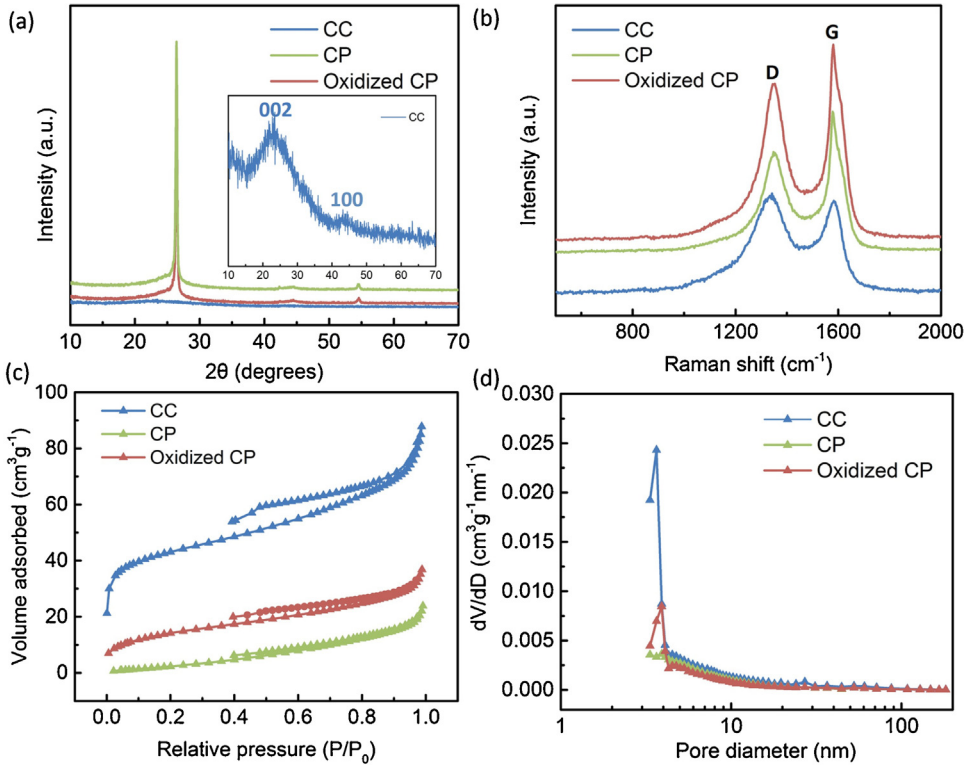

Fig. 3. XRD patterns (a), Raman spectra (b), N_2 adsorption/desorption isotherms (c) and pore size distribution (d) of CP, oxidized CP and CC.

indicative of the formation of mesoporous structure [48]. The BET specific surface area of CC electrode ($16.6\,m^2\,g^{-1}$) is much larger than that of CP ($1.2\,m^2\,g^{-1}$) and oxidized CP ($5.2\,m^2\,g^{-1}$), confirming the high porosity of CC. Two apparent peaks at ~4 and ~28 nm are observed in Fig. 3d for CC electrode, which are well within the mesoporous range. Therefore, this porous structure and high surface area of CC electrode reduce the mass transport resistance of the electrolytes and provide plenty of active sites for redox reactions.

The surface chemistry of the three types of electrodes was investigated with X-ray photoelectron spectroscopy (XPS). The results are presented in Fig. 4, where all spectra are calibrated by the C1s peak of carbon at 284.5 eV [30]. The O1s peak for CC electrode at the binding energy of 532 eV shows much higher intensity than that of untreated CP and oxidized CP, owing to the retained oxygen-containing species after the pyrolysis process. The high-resolution spectra and peak fittings of C1s and O1s are carried out to identify the composition of each functional group and the corresponding ratio, as illustrated in Fig. 4b and c. It can be seen that the untreated CP shows a sharp graphitic carbon (sp^2 C=C) peak at 284.3 eV and an obvious sp^3-bonded carbon peak at 285.1 eV appears for the oxidized carbon paper [49], whereas the corresponding high-resolution C1s spectra for CC electrode exhibits obvious sp^3 C—C and C—O (286 eV) peaks due to the presence of amorphous carbon and functional groups [50]. The O1s peaks in Fig. 4c at 530.6, 531.5 and 532.9 eV [30] can be attributed to C=O, C—OH and C—C=O, respectively. The untreated and oxidized CP electrodes only show two weak peaks of C-OH and C—C=O, while three independent and strong peaks can be observed clearly for CC, indicating the presence of large amounts of C=O, C-OH and C—C=O functional groups on the surface.

Surface wettability was also evaluated through the contact angle of water on the electrode surface. As observed in Fig. 5, both the CP and oxidized CP have the highly hydrophobic surface with contact angles of more than 90°. The contact angle of oxidized CP is slightly smaller than that of untreated CP, ascribing to the introduction of hydrophilic functional groups during the thermal treatment process. By comparison, the water droplet on the CC is soaked instantly as long as it is dropped on the surface, suggesting the good wettability of CC electrode. As a result, the CC electrode with a large surface area and highly hydrophilic surface ensures the fast diffusion of electrolyte and provides abundant active sites to improve the kinetics of vanadium redox reaction, which are favorable to enhance the performance of the battery [23].

Cyclic voltammetry tests were performed on the three-electrode system to evaluate the electrochemical activity of CC, CP and oxidized CP electrodes. The CV curves of three electrodes at the scan rate of $5\,mVs^{-1}$ are shown in Fig. 6a. Two main peaks corresponding to the VO^{2+}/VO_2^+ redox reaction are observed in all curves, stating that this redox reaction is a typical quasi-reversible process. The peak separation of potential ($\Delta E = E_{pa}\text{-}E_{pc}$), anodic ($I_{pa}$) and cathodic peak current (I_{pc}) are used to estimate the reversibility of vanadium redox reaction. The oxidized CP electrode shows a potential separation of 256 mV, slighter lower than that for pristine CP (278 mV). By contrast, the potential separation for the CC electrode is 180 mV, almost 100 mV lower than the pristine CP electrode, indicating a reduction in mass transport and charge transfer resistance resulting from the hydrophilic surface with oxygen functional groups. Besides, the CC electrode exhibits the highest anodic and cathodic peak currents of 13.36 mA and 10.57 mA, larger than that for oxidized CP (I_{pa} = 11.63 mA and I_{pc} = 9.34 mA) and pristine CP (I_{pa} = 9.34 mA, I_{pc} = 7.85 mA), owing to

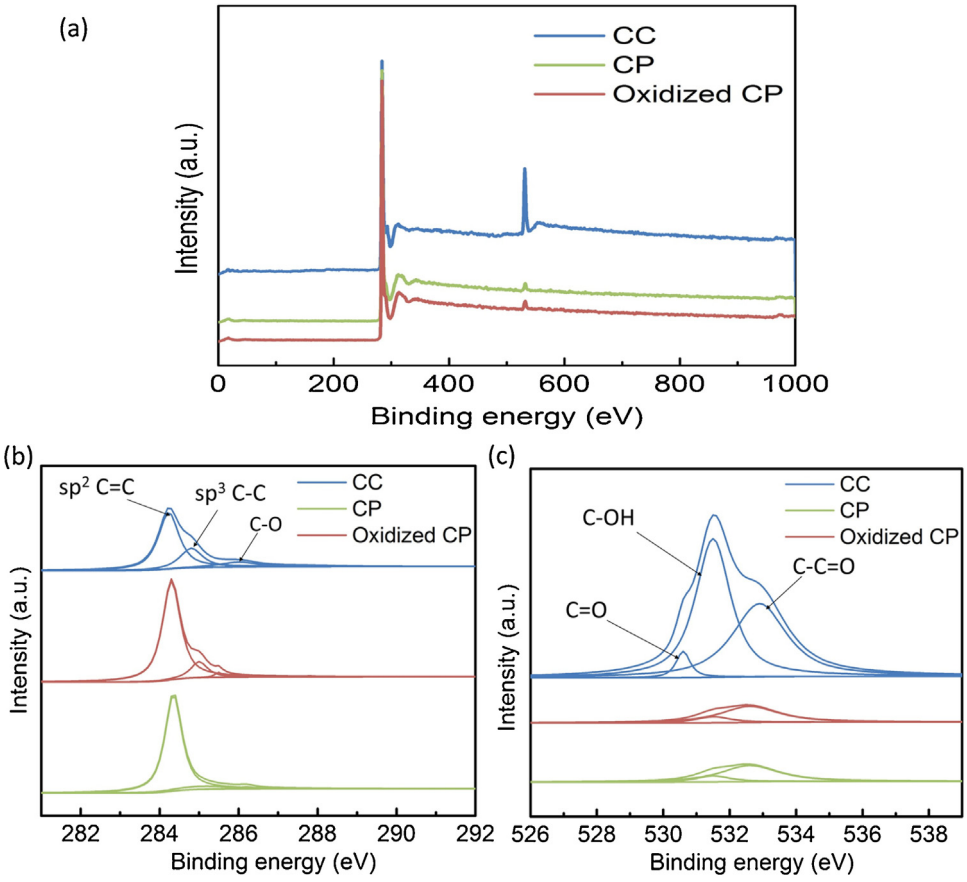

Fig. 4. (a) XPS survey of the CC, CP and oxidized CP electrodes. XPS analysis and its fitting from high resolution (b) C1s peak, (c) O1s peak.

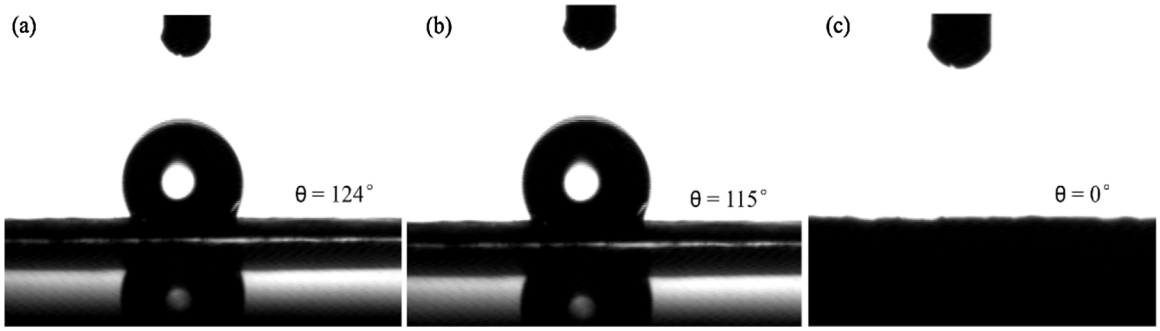

Fig. 5. Contact angle measurement of (a) CP (b) oxidized CP and (c) CC.

the higher specific area and plentiful catalytic functional groups. The CV tests of CC electrode with different scan rates from 5 mV s^{-1} to 50 mV s^{-1} are presented in Fig. 6b. The mass transfer property can be assessed by plotting the peak current *versus* the square root of scan rate. The value of the coefficient of determination (R^2) in the inset figure in Fig. 6c is 99.98%, implying that a diffusion process controls the vanadium redox reaction on the electrode. The electrochemical impedance spectra (EIS) recorded in 1 M $VOSO_4$ + 3 M H_2SO_4 solution at the open circuit potential are shown in Fig. 6d. The Nyquist plot consists of a semicircle part at high-frequency region and a linear part at the low-frequency region, associated with the charge transfer process occurring at the electrolyte/electrode interface and the vanadium ion diffusion through solutions [51,52]. The oxidized CP electrode shows much smaller charge transfer resistance than CP does due to the improved activity through thermal treatment, and the CC electrode exhibits the smallest semi-circle at high-frequency region and more vertical line at low-frequency region. The lower charge transfer resistance and faster mass transfer process are achieved on CC electrode ascribing to the abundant exposed active sites and lower surface energy induced by the functional groups, which agree well with the results of the cyclic voltammetry tests.

To further demonstrate the practical application of the prepared electrodes, three single cells were assembled with pristine CP, oxidized CP and the CC electrodes respectively to evaluate the electrochemical performance. The charge/discharge cycling tests were performed within the current density from 40 to 100 mA cm^{-2}. The voltage profiles of the oxidized CP and CC electrodes at various current densities are shown in Fig. 7a and b, respectively. It is observed the CC electrode presents a lower charge and higher discharge plateaus than oxidized CP electrode due to the lower overpotentials, suggesting that the defects and functional groups on CC surface have greatly enhanced the electrochemical activity for redox reaction and improved the performance of VRFB.

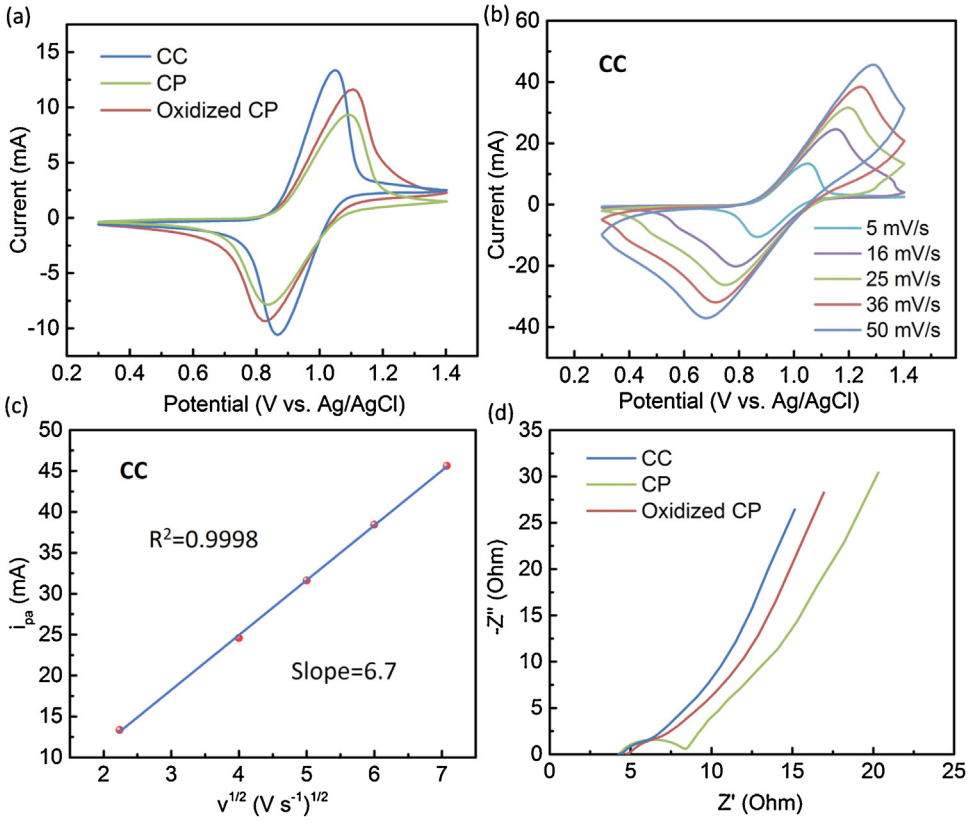

Fig. 6. (a) Cyclic voltammograms (CV) of the CC, CP and oxidized CP at a scan rate of 5 mV s^{-1} with a potential window of 0.3 to 1.4 V *versus* Ag/AgCl, (b) CV of the CC electrode at different scan rates, (c) The fit line of pear current *versus* the square root of scan rate for CC electrode, (d) Nyquist plots of CC, CP and oxidized CP in the frequency range from 10^{-2} to 10^5 Hz in 1 M $VOSO_4$ + 3 M H_2SO_4 solution at open circuit potential.

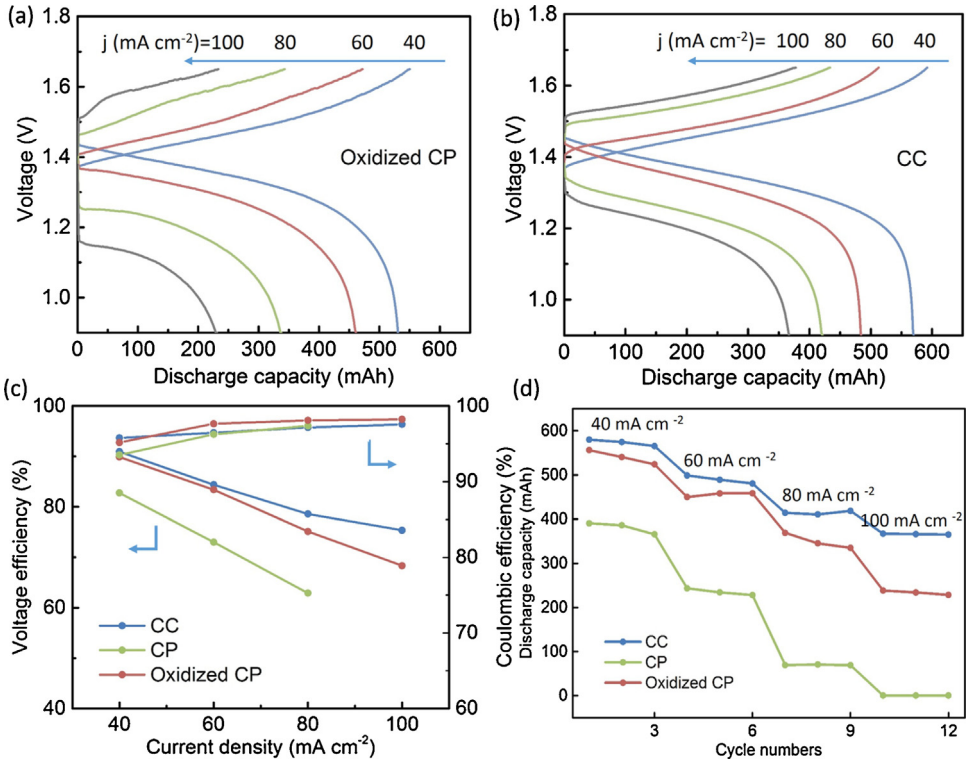

Fig. 7. Charge-discharge curves of VRFBs with (a) oxidized CP electrode and (b) CC electrode at various current densities; (c) Coulombic and voltage efficiencies of VRFBs with various electrodes; (d) Discharge capacity of VRFBs as a function of cycle number at different current densities.

Correspondingly, the battery with CC electrode exhibits longer charge/discharge time and achieves higher discharge capacity. At the current density of 100 mA cm^{-2}, the VRFB with CC electrode presents a discharge capacity of 366 mAh, more than 100 mAh higher than that for oxidized CP.

The coulombic efficiency (CE) and voltage efficiency (VE) are obtained from the ratio of discharge/charge capacity and discharge/charge voltage, respectively. The three batteries with various electrodes present close CEs, which increase from approximately 95% to 98% within the current density range from 40 to 100 mA cm^{-2}, as illustrated in Fig. 7c. However, the VE of the battery with CC electrodes is the highest among three batteries, particularly at high current densities, stating that the voltage efficiency is highly dependent on the electrochemical activity and surface chemistry of the electrode. The VE of the battery with CC electrode ranges from 91% to 75.4% with current density increasing from 40 to 100 mA cm^{-2}, higher than that for oxidized CP electrode (from 90% to 68.3%). Remarkably, the VE of CC electrode is more than ten percent higher than that of pristine CP, and it is notable that VRFB with the pristine CP electrode is even incapable of working within the given voltage range at 100 mA cm^{-2} due to its poor electrochemical activity. Therefore the high voltage efficiency of CC electrode can be attributed to the large amounts of active sites and catalytic effect of oxygen functional groups. Fig. 7d shows the plot of discharge capacities of various batteries as a function of cycle number under various current densities. The capacity declines due to the increasd overpotential with the increasing current density. It is seen that the battery with CC electrode exhibits the highest discharge capacity under all current densities, attributing to the excess surface functional groups and excellent hydrophicity. Moreover, the VRFB with CC electrode presents the best capacity retention by delivering the discharge capacity from 580 mAh to 366 mAh within the current density range from 40 to 100 mA cm^{-2}. In contrast, the battery with oxidized CP only provides 228 mAh at 100 mA cm^{-2} and the pristine CP could not even work at this current density.

Then cycling tests were performed to investigate the stability of flow batteries with various electrodes. The energy efficiencies illustrated in Fig. 8 shows the battery with CC electrode achieves the highest EE from 87.1% to 74% within the current density range from 40 to 100 mA cm^{-2}. When the current density is switched from 100 to 40 mA cm^{-2}, the energy efficiency of the battery with CC electrode recovers from 74% to 86.3%, much higher than that of CP (77.9%) and oxidized CP electrodes (84.2%). During the cycling test, the battery with CC electrodes shows a steady trend and retains the highest energy efficiency at the end of the test, demonstrating the robustness and chemical stability of the

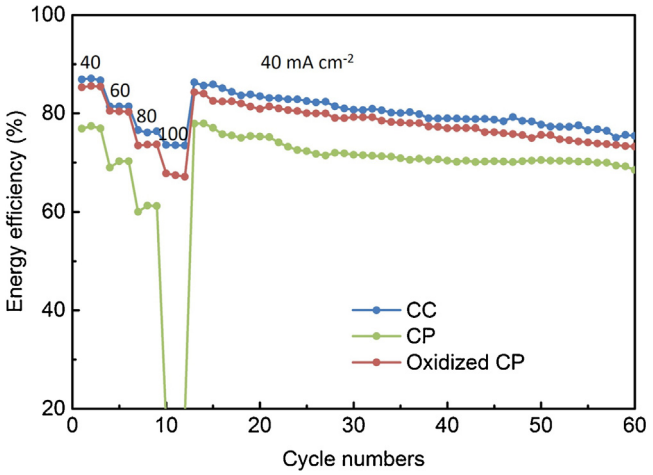

Fig. 8. Energy efficiencies of CC, CP and oxidized CP electrodes during cycling test.

prepared electrodes. Overall, the battery with CC electrodes exhibits the best performance with respect to the VE, EE, rate capability and stability due to the fast mass transfer and good reaction kinetics resulting from the large amounts of active sites and oxygen-containing species in the carbonized cotton surface.

4. Conclusions

In summary, the biomass-derived electrodes were synthesized from low-cost and environmental benign cotton by a simple one-step pyrolysis method and applied to a VRFB for the first time. The CC electrode possessed a large surface area, excellent hydrophilicity and abundant functional groups, therefore while applied in VRFB it provided a fast electrolyte diffusion rate, adequate active sites and exhibited excellent catalytic activity towards vanadium redox reactions. The battery with CC electrode exhibited an energy efficiency of 73.5% and discharge capacity of 366 mAh at a current density of 100 mA cm^{-2}, much higher than that of oxidized CP electrode (67%, 234 mAh). Moreover, the VRFB with CC electrode provided the highest discharge capacity under various current densities, and achieved the best rate capability ascribing to the large surface area and abundant active sites. Therefore, this study has demonstrated the successful application of cotton-derived electrodes in VRFB system and showed great promise of biomass derived material for high-performance VRFBs.

Acknowledgement

The work described in this paper was fully supported by a grant from the Research Grants council of the Hong Kong Special Administrative Region, China (Project No. 623313).

References

[1] B. Dunn, H. Kamath, J. Tarascon, Electrical energy storage for the grid: a battery of choices, Science 928 (2012).
[2] B. Vad, H. Lund, K. Karlsson, 100% Renewable energy systems, climate mitigation and economic growth, Appl. Energy 88 (2015) 488–501.
[3] Z. Yang, J. Zhang, M.C.W. Kintner-meyer, X. Lu, D. Choi, J.P. Lemmon, Electrochemical energy storage for green grid.pdf, Chem. Rev. (2011) 3577–3613.
[4] J. Liu, J.G. Zhang, Z. Yang, J.P. Lemmon, C. Imhoff, G.L. Graff, L. Li, J. Hu, C. Wang, J. Xiao, G. Xia, V.V. Viswanathan, S. Baskaran, V. Sprenkle, X. Li, Y. Shao, B. Schwenzer, Materials science and materials chemistry for large scale electrochemical energy storage: from transportation to electrical grid, Adv. Funct. Mater. 23 (2013) 929–946.
[5] M. Skyllas-Kazacos, M.H. Chakrabarti, S. a. Hajimolana, F.S. Mjalli, M. Saleem, Progress in flow battery research and development, J. Electrochem. Soc. 158 (2011) R55.
[6] L. Li, S. Kim, W. Wang, M. Vijayakumar, Z. Nie, B. Chen, J. Zhang, G. Xia, J. Hu, G. Graff, J. Liu, Z. Yang, A stable vanadium redox-flow battery with high energy density for large-scale energy storage, Adv. Energy Mater. 1 (2011) 394–400.
[7] B. Li, M. Gu, Z. Nie, Y. Shao, Q. Luo, X. Wei, X. Li, J. Xiao, C. Wang, V. Sprenkle, W. Wang, Bismuth nanoparticle decorating graphite felt as a high-performance electrode for an all-vanadium redox flow battery, Nano Lett. 13 (2013) 1330–1335.
[8] S.M. Park, J.H. Kim, M. Skyllas-kazacos, As featured in, J. Mater. Chem. A: Mater. Energy Sustain. 3 (2015) 16913–16933.
[9] X. Li, K. Huang, S. Liu, N. Tan, L. Chen, Characteristics of graphite felt electrode electrochemically oxidized for vanadium redox battery application, Trans. Nonferrous Met. Soc. China 17 (2007) 195–199.
[10] A. Parasuraman, T.M. Lim, C. Menictas, M. Skyllas-Kazacos, Review of material research and development for vanadium redox flow battery applications, Electrochim. Acta 101 (2013) 27–40.
[11] H. Kaneko, K. Nozaki, Y. Wada, T. Aoki, A. Negishi, M. Kamimoto, Vanadium redox reactions and carbon electrodes for vanadium redox flow battery, Electrochim. Acta 36 (1991) 1191–1196.
[12] K.J. Kim, M.-S. Park, Y.-J. Kim, J.H. Kim, S.X. Dou, M. Skyllas-Kazacos, A technology review of electrodes and reaction mechanisms in vanadium redox flow batteries, J. Mater. Chem. A 3 (2015) 16913–16933.
[13] L. Yue, W. Li, F. Sun, L. Zhao, L. Xing, Highly hydroxylated carbon fibres as electrode materials of all-vanadium redox flow battery, Carbon N. Y. 48 (2010) 3079–3090.
[14] V. Viswanathan, A. Crawford, D. Stephenson, S. Kim, W. Wang, B. Li, G. Coffey, E. Thomsen, G. Graff, P. Balducci, M. Kintner-Meyer, V. Sprenkle, Cost and performance model for redox flow batteries, J. Power Sources 247 (2014) 1040–1051.
[15] C. Ding, H. Zhang, X. Li, T. Liu, F. Xing, Vanadium flow battery for energy storage: prospects and challenges, J. Phys. Chem. Lett. 4 (2013) 1281–1294.
[16] A. Di Blasi, O. Di Blasi, N. Briguglio, A.S. Aricò, D. Sebastián, M.J. Lázaro, G. Monforte, V. Antonucci, Investigation of several graphite-based electrodes for vanadium redox flow cell, J. Power Sources 227 (2013) 15–23.
[17] K.-L. Huang, X. Li, S. Liu, N. Tan, L. Chen, Research progress of vanadium redox flow battery for energy storage in China, Renew. Energy 33 (2008) 186–192.
[18] B. Sun, M. Skyllas-Kazacos, Modification of graphite electrode materials for vanadium redox flow battery application—I. Thermal treatment, Electrochim. Acta 37 (1992) 1253–1260.
[19] B. Sun, M. Skyllas-Kazacos, Chemical modification of graphite electrode materials for vanadium redox flow battery application—part II. Acid treatments, Electrochim. Acta 37 (1992) 2459–2465.
[20] W. Zhang, J. Xi, Z. Li, H. Zhou, L. Liu, Z. Wu, X. Qiu, Electrochemical activation of graphite felt electrode for VO 2+/VO2+ redox couple application, Electrochim. Acta 89 (2013) 429–435.
[21] M.A. Goulet, M. Skyllas-Kazacos, E. Kjeang, The importance of wetting in carbon paper electrodes for vanadium redox reactions, Carbon N. Y. 101 (2016) 390–398.
[22] K.J. Kim, Y.J. Kim, J.H. Kim, M.S. Park, The effects of surface modification on carbon felt electrodes for use in vanadium redox flow batteries, Mater. Chem. Phys. 131 (2011) 547–553.
[23] L. Industry, F. Sciences, ZrO2 Nanoparticles modified graphite felt: bifunctional ZrO2 nanoparticles modified graphite felt: bifunctional effects on vanadium flow, Batteries (2016) 2–11.
[24] P. Han, Y. Yue, Z. Liu, W. Xu, L. Zhang, H. Xu, S. Dong, G. Cui, E. Sum, M. Rychcik, M. Skyllas-kazacos, Graphene oxide nanosheets/multi-walled carbon nanotubes hybrid as an excellent electrocatalytic material towards VO2+/VO2 + redox couples for vanadium redox flow batteries, Energy Environ. Sci. 4 (2011) 4710.
[25] P. Han, H. Wang, Z. Liu, X. Chen, W. Ma, J. Yao, Y. Zhu, G. Cui, Graphene oxide nanoplatelets as excellent electrochemical active materials for VO2+/VO2+ and V2+/V3+ redox couples for a vanadium redox flow battery, Carbon N. Y. 49 (2011) 693–700.
[26] Z. González, C. Botas, C. Blanco, R. Santamaría, M. Granda, P. Álvarez, R. Menéndez, Graphite oxide-based graphene materials as positive electrodes in vanadium redox flow batteries, J. Power Sources 241 (2013) 349–354.
[27] W. Li, J. Liu, C. Yan, Modified multiwalled carbon nanotubes as an electrode reaction catalyst for an all vanadium redox flow battery, J. Solid State Electrochem. 17 (2013) 1369–1376.
[28] W. Li, J. Liu, C. Yan, Multi-walled carbon nanotubes used as an electrode reaction catalyst for VO2+/VO2+ for a vanadium redox flow battery, Carbon N. Y. 49 (2011) 3463–3470.
[29] G. Wei, C. Jia, J. Liu, C. Yan, Carbon felt supported carbon nanotubes catalysts composite electrode for vanadium redox flow battery application, J. Power Sources 220 (2012) 185–192.
[30] M. Park, Y.J. Jung, J. Kim, H. Il Lee, J. Cho, Synergistic effect of carbon nanofiber/nanotube composite catalyst on carbon felt electrode for high-performance all-vanadium redox flow battery, Nano Lett. 13 (2013) 4833–4839.
[31] K.J. Kim, M.-S. Park, J.-H. Kim, U. Hwang, N.J. Lee, G. Jeong, Y.-J. Kim, Novel catalytic effects of Mn3O4 for all vanadium redox flow batteries, Chem. Commun. 48 (2012) 5455.
[32] B. Li, M. Gu, Z. Nie, X. Wei, C. Wang, V. Sprenkle, W. Wang, Nanorod niobium oxide as powerful catalysts for an all vanadium redox flow battery, Nano Lett. 14 (2014) 158–165.
[33] C. Yao, H. Zhang, T. Liu, X. Li, Z. Liu, Carbon paper coated with supported tungsten trioxide as novel electrode for all-vanadium flow battery, J. Power Sources 218 (2012) 455–461.
[34] L. Wei, T. Zhao, L. Zeng, X. Zhou, Y. Zeng, Titanium carbide nanoparticle-decorated electrode enables significant enhancement in performance of all-vanadium redox flow batteries, Energy Technol. (2016) 1–8.
[35] H. Zhou, J. Xi, Z. Li, Z. Zhang, L. Yu, L. Liu, X. Qiu, L. Chen, RSC Advances performance electrode for vanadium redox fl ow, RSC Adv. 4 (2014) 61912–61918.
[36] C. Busacca, O. Di Blasi, N. Briguglio, M. Ferraro, V. Antonucci, A. Di Blasi, Electrochimica Acta Electrochemical performance investigation of electrospun urchin-like V2O3 – CNF composite nanostructure for vanadium redox fl ow battery, Electrochim. Acta 230 (2017) 174–180.
[37] A. Di Blasi, C. Busaccaa, O. Di Blasia, N. Briguglioa, G. Squadritoa, V. Antonuccia, Synthesis of flexible electrodes based on electrospun carbon nanofibers with Mn3O4 nanoparticles for vanadium redox flow battery application, Appl. Energy 190 (2017) 165–171.
[38] M. Pasta, F. la Mantia, L. Hu, H.D. Deshazer, Y. Cui, Aqueous supercapacitors on conductive cotton, Nano Res. 3 (2010) 452–458.
[39] D. Oh, J. Qi, Y.-C. Lu, Y. Zhang, Y. Shao-Horn, A.M. Belcher, Biologically enhanced cathode design for improved capacity and cycle life for lithium-oxygen batteries, Nat. Commun. 4 (2013) 2756.
[40] J. Xue, Y. Zhao, H. Cheng, C. Hu, Y. Hu, Y. Meng, H. Shao, Z. Zhang, L. Qu, An all-cotton-derived, arbitrarily foldable, high-rate, electrochemical supercapacitor, Phys. Chem. Chem. Phys. 15 (2013) 8042.
[41] K. Song, W.-L. Song, L.-Z. Fan, Scalable fabrication of exceptional 3D carbon networks for supercapacitors, J. Mater. Chem. A 00 (2015) 1–8.

[42] A. Jain, R. Balasubramanian, M.P. Srinivasan, Hydrothermal conversion of biomass waste to activated carbon with high porosity: a review, Chem. Eng. J. 283 (2016) 789–805.
[43] C. Péan, C. Merlet, B. Rotenberg, P.A. Madden, P.L. Taberna, B. Daffos, M. Salanne, P. Simon, Hierarchically porous carbon derived from polymers and biomass: effect of interconnected pores on energy applications, Energy Environ. Sci. 8 (2014) 1576–1583.
[44] M. Ulaganathan, A. Jain, V. Aravindan, S. Jayaraman, W.C. Ling, T.M. Lim, M.P. Srinivasan, Q. Yan, S. Madhavi, Bio-mass derived mesoporous carbon as superior electrode in all vanadium redox flow battery with multicouple reactions, J. Power Sources 274 (2015) 846–850.
[45] M. Park, J. Ryu, Y. Kim, J. Cho, Corn protein-derived nitrogen-doped carbon materials with oxygen-rich functional groups: a highly efficient electrocatalyst for all-vanadium redox flow batteries, Energy Environ. Sci. 7 (2014) 3727–3735.
[46] A.C. Ferrari, D.M. Basko, Raman spectroscopy as a versatile tool for studying the properties of graphene, Nat. Nanotechnol. 8 (2013) 235–246.
[47] F. Tuinstra, L. Koenig, Raman Spectrum of Graphite, J. Chem. Phys. 53 (1970) 1126–1130.
[48] B. Xu, H. Duan, M. Chu, G. Cao, Y. Yang, Facile synthesis of nitrogen-doped porous carbon for supercapacitors, J. Mater. Chem. A. 1 (2013) 4565.
[49] S. Osswald, G. Yushin, V. Mochalin, S.O. Kucheyev, Y. Gogotsi, Control of sp2/sp3 carbon ratio and surface chemistry of nanodiamond powders by selective oxidation in air, J. Am. Chem. Soc. 128 (2006) 11635–11642.
[50] C. Gao, N. Wang, S. Peng, S. Liu, Y. Lei, X. Liang, S. Zeng, H. Zi, Influence of Fenton's reagent treatment on electrochemical properties of graphite felt for all vanadium redox flow battery, Electrochim. Acta 88 (2013) 193–202.
[51] J.P. Meyers, M. Doyle, R.M. Darling, J. Newman, The Impedance Response of a Porous Electrode Composed of Intercalation Particles, J. Electrochem. Soc. 147 (2000) 2930.
[52] H. Cui, G. Zhu, X. Liu, F. Liu, Y. Xie, C. Yang, T. Lin, H. Gu, F. Huang, Niobium Nitride Nb_4N_5 as a New High-Performance Electrode Material for Supercapacitors, Adv. Sci. (2015).